

## P5.5

# CHANNEL SELECTION FOR THE NEXT GENERATION GEOSTATIONARY ADVANCED IMAGERS

Timothy J. Schmit

NOAA/NESDIS, Office of Research and Applications, Advanced Satellite Products Team (ASPT)

W. Paul Menzel

NOAA/NESDIS, Office of Research and Applications

Mathew M. Gunshor, James P. Nelson III

Cooperative Institute for Meteorological Satellite Studies (CIMSS)

University of Wisconsin-Madison

Madison, WI

## 1. INTRODUCTION

To keep pace with the growing need for GOES data and products, NOAA is evolving its geostationary sensor capabilities. The Advanced Baseline Imager (ABI) will be the next generation geostationary imager on GOES-R, beginning in 2010. As with the current GOES Imager, this instrument will be used for a wide range of both qualitative and quantitative applications. The ABI will include a number of improvements over the existing imager besides the additional bands. The ABI will improve the spatial coverage from nominally 4 to 2 km for the infrared bands, as well as almost a five-fold increase of the coverage rate (Gurka and Dittberner 2001). This imager will have a minimum of eight spectral bands and a maximum of twelve spectral bands. The minimum eight bands are similar to the five bands on the current GOES-8/11 Imagers (Menzel and Purdom 1994), plus a snow/cloud-discriminating 1.6  $\mu\text{m}$  band, a mid-tropospheric 7.0  $\mu\text{m}$  water vapor band, and a 13.3  $\mu\text{m}$  band useful for determining cloud heights and amounts. This carbon dioxide-sensitive band is similar to that on the GOES-M and beyond series of Imagers (Schmit et al. 2001). The ABI bands were selected after considering NWS requirements, existing bands on the GOES Imagers and Sounders, bands on other future geostationary satellites, and bands on current and future polar-orbiting satellites. For example, the next generation METEOSAT (METEOrological SATellite) Second Generation (MSG), to be launched in 2002, will have 12 channels, including two water vapor channels centered at 6.2 and 7.3  $\mu\text{m}$  (Schmetz et al. 1998).

The uses of the eight core bands, and the four additional bands, are briefly described in the following section.

---

*Corresponding author address:* Timothy J. Schmit, 1225 West Dayton Street, Madison, WI 53706; email: Tim.J.Schmit@noaa.gov.

## 2. ABI CHANNEL SELECTION

The 0.64  $\mu\text{m}$  visible band is used for: daytime cloud imaging; snow and ice cover; detection of severe weather onset detection; low-level cloud drift winds; fog; smoke; volcanic ash, hurricane analysis; and winter storm analysis.

During the day, the 1.6  $\mu\text{m}$  band can be used for: cloud/snow/ice discrimination; total cloud cover; aviation weather analyses for cloud-top phase (Hutchison 1999); and detecting smoke from low-burn-rate fires.

The shortwave IR window (3.9  $\mu\text{m}$ ) band has many uses: fog (Ellrod et al. 1998) and low-cloud discrimination at night; fire identification (Prins et al., 1998); volcanic eruption and ash detection; and daytime reflectivity for snow/ice.

The 6.15  $\mu\text{m}$  and 7.0  $\mu\text{m}$  bands will be used for upper and mid-tropospheric water vapor tracking; jet stream identification (Weldon et al., 1991); hurricane track forecasting; mid-latitude storm forecasting; severe weather analysis and for estimating upper level moisture (Soden et al., 1993; Moody et al., 1999).

The longwave infrared window (11.2  $\mu\text{m}$ ) band will provide day/night cloud analyses for general forecasting and broadcasting applications; precipitation estimates (Vicente et al., 1998); severe weather analyses; cloud drift winds (Velden et al. 1998a); hurricane strength (Velden et al. 1998b) and track analyses; cloud top heights; volcanic ash detection (Prata 1989); fog detection (in multi-band products); winter storms; and cloud phase/particle size estimates (in multi-band products).

The 12.3  $\mu\text{m}$  band will offer nearly continuous cloud monitoring for numerous applications; low-level moisture determinations; volcanic ash identification detection (Davies and Rose 1998); Sea Surface Temperature measurements (Wu et al. 1999) and cloud particle size (in multi-band products).

The 13.3  $\mu\text{m}$  band will be used for cloud top height assignments for cloud-drift winds;

cloud products for ASOS supplement (Schreiner et al. 1993; Wylie and Menzel 1999); tropopause delineation; and estimating cloud opacity.

Four bands have been proposed as additions to the core eight, with the goal of meeting NWS requirements and enhancing many products/applications. The 8.5  $\mu\text{m}$  band, in conjunction with the 11.2  $\mu\text{m}$  band, will enable detection of volcanic dust cloud containing sulfuric acid aerosols (Realmuto et al. 1997; Baran et al. 1993; Ackerman and Strabala 1994). In addition, the 8.5  $\mu\text{m}$  band can be combined with the 11.2 and 12.3  $\mu\text{m}$  bands to derive cloud phase (Strabala et al. 1994).

The 10.35  $\mu\text{m}$  band will help to derive low-level moisture, cloud particle size and surface properties. Chung et al. (2000) showed how the 10 - 11  $\mu\text{m}$  region is important for determining particle sizes of ice-clouds.

A visible band at 0.86  $\mu\text{m}$  will help the detection of aerosols and vegetation. Characterizing aerosols and their optical properties is essential for improving a number of satellite products, for example land and sea surface temperatures. This band may enable localized vegetation stress monitoring, fire danger monitoring, and albedo retrieval. Other applications include suspended sediment detection (Aquirre-Gomez, 2000).

Finally, a near-infrared channel at 1.38  $\mu\text{m}$  is proposed to detect very thin cirrus not detected by other bands. The 1.38  $\mu\text{m}$  band is similar to a band on MODIS (MODerate resolution Imaging Spectroradiometer). Radiation from this band does not sense into the lower troposphere due to water vapor absorption and thus it provides excellent daytime sensitivity to very thin cirrus.

The spectral widths of the ABI infrared bands are shown both in Table 1 and Fig. 1. A number of these same bands were selected by NASA for the Advanced Geosynchronous Studies Imager (AGSI) (Hinkal et al. 1999).

Table 1. ABI channel selection. The four shaded bands denote the proposed additional bands.

| Wavelength ( $\mu\text{m}$ ) | Description    |
|------------------------------|----------------|
| 0.64 +/- 0.05                | Visible        |
| 0.86 +/- 0.05                | Visible        |
| 1.375 +/- 0.015              | Near IR        |
| 1.61 +/- 0.03                | Near IR        |
| 3.9 +/- 0.1                  | Shortwave IR   |
| 6.15 +/- 0.45                | Water Vapor 1  |
| 7.0 +/- 0.2                  | Water Vapor 2  |
| 8.5 +/- 0.2                  | IR Window 1    |
| 10.35 +/- 0.25               | IR Window 2    |
| 11.2 +/- 0.4                 | IR Window 3    |
| 12.3 +/- 0.5                 | IR Window 4    |
| 13.3 +/- 0.3                 | Carbon Dioxide |

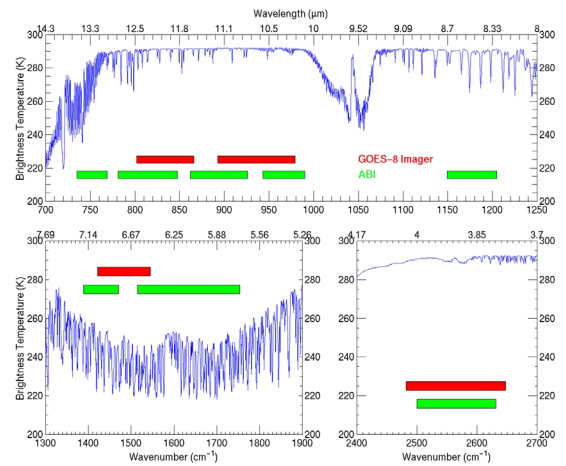


Fig. 1 The GOES-8 IR spectral bands (top bars) and the ABI IR spectral bands (lower bars). A high-spectral resolution earth-emitted spectra is also plotted.

The corresponding ABI weighting functions (for the IR bands) are shown in Fig. 2.

### 3. ABI SIMULATIONS BASED ON MODIS DATA

There are two main methods to simulate the expected signal from a future instrument. One method uses a radiative transfer model along with some estimate of the state of the atmosphere to calculate the expected (noise free) signal and then add noise. The second method, employed in this study, is to use higher-resolution data to simulate ABI. This method allows for more realistic simulations, especially of the clouds. Bands on the high-spatial resolution NASA MODIS data (Ackerman et al. 1998) have been used to simulate the ABI bands. The 10.35  $\mu\text{m}$  band could not be simulated since there is no corresponding MODIS band.

The simulation of the ABI from MODIS data consists of two steps. First, apply a point spread function (PSF) to the MODIS data to account for diffraction and other blurring affects. PSF data were obtained from MIT/Lincoln Labs (personal communication, Edward Wack). Second, remap the MODIS 1 km to the ABI 2 km spatial resolution. No corrections were made to account for different spectral response functions between MODIS and ABI. Also, given the similarities between MODIS and ABI bit depth and instrument noise, no adjustments were made for either parameter.

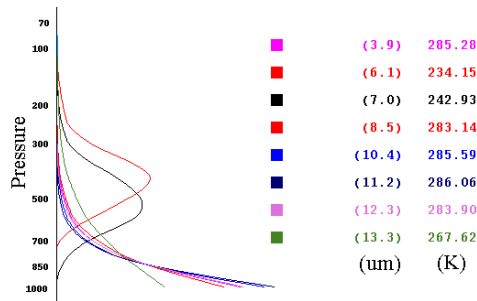


Fig. 2. The contribution weighting functions are plotted for each of the IR ABI bands for the standard atmosphere at a 40 degree local zenith angle.

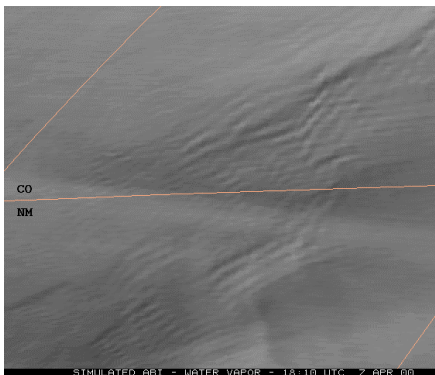
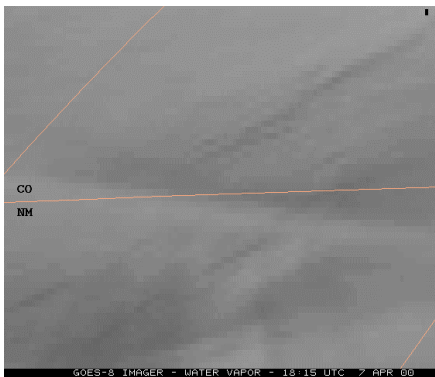


Fig. 3. Actual GOES Imager water vapor image (top) and the simulated ABI image (bottom). Both images are shown in the GOES projection. The gravity waves are clearly depicted in the ABI image. This case is from 7 April 2000, 1815 UTC.

Figure 3 shows current GOES and simulated ABI (from MODIS imagery) water vapor images in cloud free skies. These mountain waves over Colorado and New Mexico were induced by strong northwesterly flow associated with a pair of upper-tropospheric jet streaks moving across the elevated terrain of the southern and central Rocky Mountains. The mountain waves appear better defined over Colorado; in fact, several aircraft reported moderate to severe turbulence over that region.

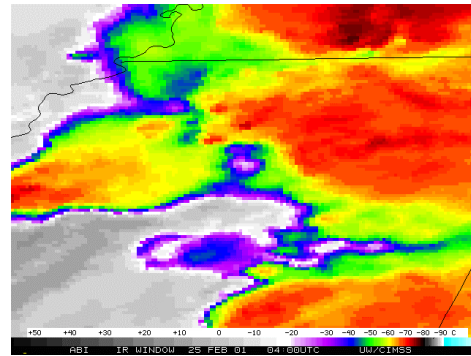
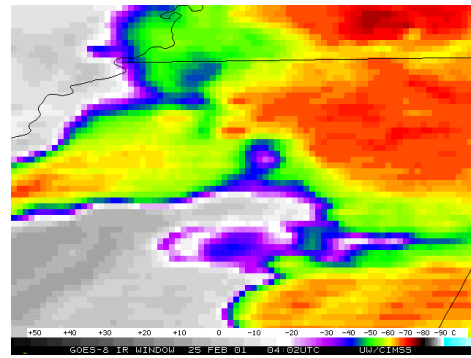


Fig. 4. Close-up of severe convection as depicted in the longwave IR window from 25 February 2001. GOES Imager (top) and simulated ABI (bottom) are shown.

Figure 4 shows GOES Imager and ABI close-ups of a severe thunderstorm. The details of the cold-tops are more evident in the ABI image. Additional comparisons are being made for a wide range of meteorological phenomena. These phenomena include wave clouds, severe convection, hurricanes, volcanoes, fires, lake ice, cloud phase and fog. For example, a thin ash plume from the Mt. Cleveland (Alaska) volcano was more readily identified in an 8.5  $\mu\text{m}$  minus 11  $\mu\text{m}$  image than in the traditional split window 11  $\mu\text{m}$  minus 12  $\mu\text{m}$  image.

#### 4. SUMMARY

The ABI represents an exciting expansion in geostationary remote sensing capabilities, especially the 12 band version. Other improvements include faster coverage and improved spatial resolution. Even with 12 bands, the instrument could benefit from the addition of two more bands, at 0.47  $\mu\text{m}$  and 9.6  $\mu\text{m}$ . The 0.47  $\mu\text{m}$  band would be used for aerosol detection and would enable daytime "true color" composites. The 9.6  $\mu\text{m}$  band would monitor total ozone on space and time scales never before possible; MSG will also have such an ozone-sensitive band. Similar bands were proposed on the AGSI (Hinkal et al. 1999).

## 5. REFERENCES

- Ackerman, S. A., K. I. Strabala, W. P. Menzel, R. A. Frey, C. C. Moeller, and L. E. Gumley, 1998: Discriminating clear sky from clouds with MODIS. *J. Geophys. Res.*, **103**, 32141-32157.
- Ackerman, S. and K. I. Strabala, 1994: Satellite remote sensing of H<sub>2</sub>SO<sub>4</sub> aerosol using the 8 to 12  $\mu$ m window region: Application to Mount Pinatubo. *J. Geo. Res.*, **99**, 18,639-18,649.
- Aquirre-Gomez, R., 2000: Detection of total suspended sediments in the North Sea using AVHRR and ship data. *Int. J. Remote Sensing*, **21**, 1583-1596.
- Baran, A. J., J. S. Foot and P. C. Dibben, 1993: Satellite detection of volcanic sulfuric acid aerosol. *Geophys. Res. Letters*, **20**, 1799-1801.
- Chung S., S. Ackerman, and P. F. van Delst, 2000: Model calculations and interferometer measurements of ice-cloud characteristics. *J. Appl. Met.*, **39**, 634-644.
- Davies, M. A., and W. I. Rose, 1998: GOES imagery fills gaps in Montserrat volcanic cloud observations. *EOS, Transactions, American Geophysical Union*, **79**, 505-507.
- Ellrod, G. P., R. V. Achutuni, J. M. Daniels, E. M. Prins, and J. P. Nelson III, 1998: An assessment of GOES-8 Imager data quality, *Bull. Amer. Meteor. Soc.*, **79**, 2509-2526.
- Gurka, J. J., and G. J. Dittberner, 2001: The next generation GOES instruments: status and potential impact. Preprint Volume. 5<sup>th</sup> Symposium on Integrated Observing Systems. 14-18 January, Albuquerque, NM, Amer. Meteor. Soc., Boston.
- Hinkal, S., Jenstrom, D.; Florez, J., Bremer, J. C.; Hersh, M.; Neuberger, D., and Kindsfather, R., 1999: Advanced Geosynchronous Studies Imager: Instrument system design. Earth Observing Systems IV, Proceedings of the Conference, Denver, CO, 18-20 July 1999. Bellingham, WA, Society of Photo-Optical Instrumentation Engineers (SPIE). SPIE Proceedings volume 3750, pp2-10.
- Hutchison, K. D., 1999: Application of AVHRR/3 imagery for improved detection of thin cirrus clouds and specification of cloud-top phase. *J. Atmos. Oceanic Tech.*, **16**, 1885-1899.
- Menzel, W. P., and J. F. W. Purdom, 1994: Introducing GOES-I: The first of a new generation of geostationary operational environmental satellites. *Bull. Amer. Meteor. Soc.*, **75**, 757-781.
- Moody J. L., A. J. Wimmers, and J. C. Davenport, 1999: Remotely sensed specific humidity: development of a derived product from the GOES Imager channel 3, *Geo. Phys. Res. Let.*, **26**, 59-62.
- Prins, E. M., J. M. Feltz, W. P. Menzel, and D. E. Ward, 1998: An overview of GOES-8 diurnal fire and smoke results for SCAR-B and 1995 fire season in South America, *J. Geophys. Res.*, **103** (D24), 31821-31835.
- Prata, A. J., 1989: Observations of volcanic ash clouds in the 10-12  $\mu$ m window using AVHRR/2 data. *Int. J. Remote Sens.*, **10**, 751-761.
- Realmuto, V. J., A. J. Sutton, T. Elias, 1997: Multispectral thermal infrared mapping of sulfur dioxide plumes: A case study from the East Rift Zone of Kilauea Volcano, Hawaii, *J. Geophys. Res.*, **102**, 15,057-15,072.
- Schmetz, J., H. Woick, S. Tjemkes, and J. Rattenborg, 1998: From Meteosat to Meteosat Second Generation, Proceedings, *Ninth Conference on Satellite Meteorology and Oceanography*, Paris, France, Amer. Meteor. Soc., 335-338.
- Schmit, T. J., E. M. Prins, T. J. Schreiner, and J. J. Gurka, 2001: Introducing the GOES-M Imager. Submitted to the *National Weather Association-Digest*.
- Schreiner, A. J., D. A. Unger, W. P. Menzel, G. P. Ellrod, K. I. Strabala, and J. L. Pellett, 1993: A comparison of ground and satellite observations of cloud cover. *Bull. Amer. Meteor. Soc.*, **74**, 1851-1861.
- Soden, B. J., and F. P. Bretherton, 1993: Upper tropospheric relative humidity from the GOES 6.7  $\mu$ m channel: Method and climatology for July 1987. *J. Geophys. Res.*, **98**, 16669-16688.
- Strabala, K. I., S. A. Ackerman, and W. P. Menzel, 1994: Cloud properties inferred from 8-12  $\mu$ m data. *J. Appl. Meteor*, **33**, 212-229.
- Velden, C. S., T. L. Olander, and S. Wanzong, 1998a: The impact of multispectral GOES-8 wind information on Atlantic tropical cyclone track forecasts in 1995. Part I: dataset methodology, description, and case analysis. *Mon. Wea. Rev.*, **126**, 1202-1218.
- Velden, C. S., T. L. Olander, and R. M. Zehr, 1998b: Development of an objective scheme to estimate tropical cyclone intensity from digital geostationary satellite infrared imagery. *Wea. Forecasting*, **13**, 172-186.
- Vicente, G. A., R. A. Scofield, and W. P. Menzel, 1998: The operational GOES infrared rainfall estimation technique, *Bull. Amer. Meteor. Soc.*, **79**, 1883-1898.
- Weldon, R. B, and S. J. Holmes, 1991: Water vapor imagery -- interpretation and applications to weather analysis and forecasting, NOAA Technical Report NESDIS 57.
- Wu, Xiangqian, W. P. Menzel, and Gary S. Wade, 1999: Estimation of sea surface temperatures using GOES-8/9 radiance measurements. *Bull. Amer. Meteor. Soc.*, **80** (6), 1127-1138.
- Wylie, D. P., and W. P. Menzel, 1999: Eight years of high cloud statistics using HIRS. *J. Climate*, **12**, 170-184.